

Steel-concrete composite bridge analysis using generalised beam theory

Rodrigo Gonçalves¹ and Dinar Camotim^{2*}

¹UNIC, Departamento de Engenharia Civil, Faculdade de Ciências e Tecnologia,
Universidade Nova de Lisboa, 2829-516 Caparica, Portugal

²ICIST/IST, Departamento de Engenharia Civil e Arquitectura, Universidade Técnica de Lisboa,
Av. Rovisco Pais, 1049-001 Lisbon, Portugal

(Received April 13, 2010, Accepted May 27, 2010)

Abstract. This paper reports recent developments concerning the application of Generalised Beam Theory (GBT) to the structural analysis of steel-concrete composite bridges. The potential of GBT-based semi-analytical or finite element-based analyses in this field is illustrated/demonstrated by showing that both accurate and computationally efficient solutions may be achieved for a wide range of structural problems, namely those associated with the bridge (i) linear (first-order) static, (ii) vibration and (iii) lateral-torsional-distortional buckling behaviours. Several illustrative examples are presented, which concern bridges with two distinct cross-sections: (i) twin box girder and (ii) twin I-girder. Allowance is also made for the presence of discrete box diaphragms and both shear lag and shear connection flexibility effects.

Keywords: steel-concrete composite bridges; generalised beam theory (GBT); cross-section deformation; thin-walled structures.

1. Introduction

Generalised Beam Theory (GBT), originally developed by Schardt (1989), is commonly viewed as an extension of Vlasov's prismatic bar theory that takes into account cross-section in-plane and out-of-plane (warping) deformation. In GBT, the beam kinematic description is based on a superimposition of pre-determined cross-section deformation modes – the functions providing their variation along the beam axis constitute the problem unknowns. This unique modal nature renders the GBT-based structural analyses considerably more efficient, versatile and “structurally illuminating” than similarly accurate finite strip or shell finite element analyses (the “classic” methods for solving thin-walled beam problems). In fact, GBT has been definitely proven to be a powerful, elegant and clarifying tool to solve a wide range of structural problems involving prismatic thin-walled members and frames (Camotim *et al.* 2004, 2006, 2010).

Following previous work by the authors (Gonçalves *et al.* 2006, 2008, 2010b), the objective of this paper is to report recent developments in the field of steel-concrete composite bridge analysis with GBT and, in particular, provide evidence that GBT constitutes a valuable and computationally efficient

* Corresponding author, Professor, E-mail: dcamotim@civil.ist.utl.pt

structural analysis method in this field (when compared with the traditional shell finite element and finite strip methods), capable of providing extremely accurate solutions for a wide range of problems. The paper focuses on the calculation of the cross-section deformation modes for steel-concrete composite open and closed multi-cell cross-sections, taking into account the presence of discrete cross-section diaphragms located along the girders, as well as making allowance for shear lag and shear connection flexibility phenomena. Several illustrative examples are presented and discussed, which concern the (i) linear (first-order) static, (ii) undamped free vibration and (iii) lateral-torsional-distortional buckling behaviours of steel-concrete composite bridges with twin box girder and twin I-girder cross-sections.

Concerning the notation adopted in the paper, vectors and matrices are indicated in **bold**. Moreover, rectangular brackets ($[]$) are used when making reference to vector/matrix components. Finally, partial derivatives are identified by subscripts following a comma, *e.g.*, if $f=f(x,y)$, then $f_{,x} = \partial f / \partial x$.

2. Brief overview of GBT

This section provides a brief overview of the GBT approach to perform structural analyses, which is included for completeness of the paper. A more in-depth description of the “classic” GBT, as well as its most recent developments, can be found the works by Schardt (1989, 1994), Davies (1998) and Camotim *et al.* (2004, 2006, 2010), and also in the references indicated therein.

Consider the arbitrary thin-walled prismatic member depicted in Fig. 1, which shows also the mid-surface axes (x, y, z) for each wall – the so-called “local” axes. According to the GBT kinematic description, Kirchhoff’s assumption is adopted (*i.e.*, fibres initially along z remain undeformed and perpendicular to the mid-surface) and, therefore, the wall displacement components, along the local axes, are given by

$$[U] = \begin{bmatrix} U_x \\ U_y \\ U_z \end{bmatrix} = \begin{bmatrix} u - z w_{,x} \\ v - z w_{,y} \\ w \end{bmatrix} \quad (1)$$

where u, v, w are the wall mid-line displacement components along x, y and z , respectively. These displacement components are expressed as

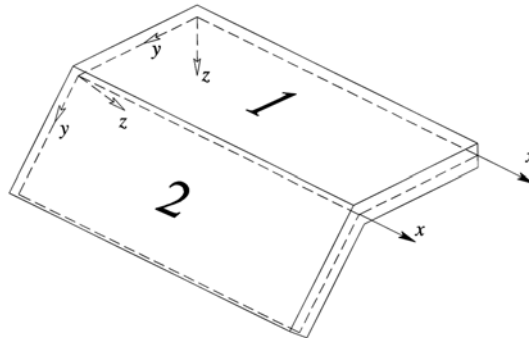


Fig. 1 Arbitrary thin-walled member local coordinate systems

$$u(x, y) = \sum_{k=1}^D \bar{u}_k(y) \phi_{k,x}(x), \quad v(x, y) = \sum_{k=1}^D \bar{v}_k(y) \phi_k(x), \quad w(x, y) = \sum_{k=1}^D \bar{w}_k(y) \phi_k(x) \quad (2)$$

where functions $\bar{u}_k(y)$, $\bar{v}_k(y)$, $\bar{w}_k(y)$ contain the mid-line displacement components associated with each of the D cross-section deformation modes and $\phi_k(x)$ are their longitudinal amplitude functions – the problem unknowns. The differentiation with respect to x appearing in $u(x, y)$ stems from the null membrane shear strain assumption ($\gamma_{xy}^M = 0$), commonly known as “Vlasov’s assumption”, which is employed in the classic GBT kinematic description and further implies that $\bar{u}_k(y) = -\bar{v}_k(y)$ (Schardt, 1989). It should be stressed that the form adopted for $u(x, y)$ in (2), although necessary to accommodate Vlasov’s assumption, does not necessarily bind the GBT approach to this assumption and, therefore, (2) may be viewed as a general kinematic description.

The kinematic assumptions (Kirchhoff’s, Vlasov’s and the assumption concerning the transverse inextensibility of the walls, which is discussed further ahead) play a key role in GBT, since they act as kinematic constraints that reduce the number of admissible cross-section deformation modes and, therefore, also reduce the number of degrees of freedom (d.o.f.) involved in the (discretised) problem. Obviously, this method/approach is only valid and useful if the assumptions adopted are acceptable for the particular problem under consideration.

The most unique feature of GBT is the identification of the functions $\bar{u}_k(y)$, $\bar{v}_k(y)$, $\bar{w}_k(y)$, which characterise the cross-section deformation modes. These functions are obtained through the performance of the so-called “GBT cross-section analysis”, which consists of two main steps:

- (i) Cross-section discretisation by means of “cross-section nodes”, with the purpose of generating an *initial* set of deformation modes (approximation functions). Each “initial” deformation mode is obtained by imposing a unit displacement (u , v or w) at a single node, while keeping all the remaining nodal displacements null. The in-plane configuration of the cross-section associated with each mode is determined through its analysis as a plane frame subjected to imposed nodal displacements, using any suitable structural analysis method (*e.g.*, direct stiffness, direct displacement or beam finite element methods).
- (ii) Performance of an appropriate change of base of the initial set of deformation modes, thus leading to a both mechanically meaningful and hierarchical set – the *final* or *orthogonal* set of deformation modes.

The authors have recently discussed and extended this cross-section analysis procedure, making it possible to analyse, more rationally, arbitrary cross-sections, namely cross-sections combining closed cells with open branches (Gonçalves *et al.* 2009, 2010b).

The stress and strain measures employed in GBT are the Green-Lagrange strains \mathbf{E} and the Second Piola-Kirchhoff stresses \mathbf{S} . Membrane and bending terms are deemed uncoupled and small strains (ϵ) are assumed for the bending terms. Although a plane strain state is automatically retrieved from the GBT kinematic description (a consequence of Kirchhoff’s assumption), a plane stress state is also assumed ($S_{zz} = S_{xz} = S_{yz} = 0$), thus leading to a (mild) inconsistency of the formulation. Moreover, in the classic GBT formulations the membrane stress field is assumed uniaxial ($S_{xx}^M \neq 0$, $S_{xy}^M = S_{yy}^M = 0$) or corresponding to “2D beam theory” ($S_{xx}^M \neq 0$, $S_{xy}^M \neq 0$, $S_{yy}^M = 0$). Since the transverse inextensibility of the walls ($\epsilon_{yy}^M = 0$) is usually assumed in either case, another (mild) inconsistency is also generated¹.

The constitutive laws adopted for the membrane and bending terms obviously depend on the assumptions made concerning the stresses. For instance, in the case of a St. Venant-Kirchhoff material law the constitutive matrices \mathbf{C} associated with (i) plane, (ii) “2D beam theory” and (iii) uniaxial (1D) stress states read

$$[\mathbf{C}_{PS}] = \begin{bmatrix} \frac{E}{1-\nu^2} & \frac{\nu E}{1-\nu^2} & 0 \\ \frac{\nu E}{1-\nu^2} & \frac{E}{1-\nu^2} & 0 \\ 0 & 0 & G \end{bmatrix}, \quad [\mathbf{C}_{2D}] = \begin{bmatrix} E & 0 & 0 \\ 0 & 0 & 0 \\ 0 & 0 & G \end{bmatrix}, \quad [\mathbf{C}_{1D}] = \begin{bmatrix} E & 0 & 0 \\ 0 & 0 & 0 \\ 0 & 0 & 0 \end{bmatrix} \quad (3)$$

where E , G and ν are the Young's modulus, shear modulus and Poisson's ratio, and vector forms of the strain and stress tensors are assumed, satisfying $\mathbf{S} = \mathbf{CE}$ and having components

$$[\mathbf{E}] = \begin{bmatrix} E_{xx} \\ E_{yy} \\ 2E_{xy} \end{bmatrix}, \quad [\mathbf{S}] = \begin{bmatrix} S_{xx} \\ S_{yy} \\ S_{xy} \end{bmatrix} \quad (4)$$

Although most GBT formulations concern elastic materials, J_2 incremental and deformation plasticity has also been covered (Gonçalves and Camotim 2004, 2007, Gonçalves *et al.* 2010a). Note that the consideration of a different constitutive model offers no major difficulty. However, the inclusion of additional strain components entails the need to incorporate associated deformation modes in the analysis, which obviously increases the number of d.o.f. involved.

The GBT equilibrium equation system is obtained from a variational principle, such as the Principle of Virtual Work. GBT-based beam finite elements are then obtained by approximating directly the deformation mode amplitude functions ϕ_k – usually by means of Hermite cubic polynomials, due to the continuity requirements stemming from Kirchhoff's assumption and the differentiation $\phi_{k,x}$ appearing in (2) (*e.g.*, Silvestre and Camotim 2003, Gonçalves and Camotim 2007). A $4D \times 4D$ element stiffness matrix is then obtained, where D is the number of deformation modes included in the analysis. However, due to the fact that $\phi_{k,x}$ is associated with $u(x,y)$, one must remove a duplicate d.o.f. for each mode involving only warping (*e.g.*, the axial extension mode). For particular problems, semi-analytical or analytical solutions may be sought, making it possible to reduce dramatically the number of d.o.f. involved, or even develop analytical or semi-analytical formulae with some practical interest (*e.g.*, Schardt 1994, Silvestre and Camotim 2004, Gonçalves *et al.* 2010a).

For example, in the context of the classic GBT, which assumes small strains and linear elastic materials, the internal virtual work may be shown to read

$$\delta W_{int} = - \int \begin{bmatrix} [\delta\phi] \\ [\delta\phi_{,x}] \\ [\delta\phi_{,xx}] \end{bmatrix}^t \begin{bmatrix} [\mathbf{B}] & [\mathbf{0}] & [\mathbf{D}_2] \\ [\mathbf{0}] & [\mathbf{D}_1] & [\mathbf{0}] \\ [\mathbf{D}_2]^t & [\mathbf{0}] & [\mathbf{C}] \end{bmatrix} \begin{bmatrix} [\phi] \\ [\phi_{,x}] \\ [\phi_{,xx}] \end{bmatrix} dx \quad (5)$$

where $[\phi]$ is a vector containing the modal amplitude functions ϕ_k and the GBT modal matrices are given by (integrations along the whole cross-section mid-line S)

¹⁾For a complete discussion on this matter, see Gonçalves *et al.* (2010b).

$$\begin{aligned}
\mathbf{B}_{ij} &= \mathbf{B}_{ij}^M + \mathbf{B}_{ij}^B = \int_S C_{22}^M t \bar{v}_{i,y} \bar{v}_{j,y} dy + \int_S \frac{C_{22}^B t^3}{12} \bar{w}_{i,yy} \bar{w}_{j,yy} dy \\
\mathbf{C}_{ij} &= \mathbf{C}_{ij}^M + \mathbf{C}_{ij}^B = \int_S C_{11}^M t \bar{u}_i \bar{u}_j dy + \int_S \frac{C_{11}^B t^3}{12} \bar{w}_i \bar{w}_j dy \\
\mathbf{D}_{1ij} &= \mathbf{D}_{1ij}^M + \mathbf{D}_{1ij}^B = \int_S C_{33}^M t (\bar{u}_{i,y} + \bar{v}_i) (\bar{u}_{j,y} + \bar{v}_j) + \int_S \frac{C_{33}^B t^3}{3} \bar{w}_{i,y} \bar{w}_{j,y} dy \\
\mathbf{D}_{2ij} &= \mathbf{D}_{2ij}^M + \mathbf{D}_{2ij}^B = \int_S C_{12}^M t \bar{v}_{i,y} \bar{u}_j dy + \int_S \frac{C_{12}^B t^3}{12} \bar{w}_{i,yy} \bar{w}_j dy
\end{aligned} \tag{6}$$

where C_{ij}^M and C_{ij}^B designate the constitutive matrix components for the membrane and bending terms, respectively, and t is the wall thickness. The above GBT modal matrices are essential to perform the mode orthogonalisation procedure leading to the final GBT cross-section deformation mode set. Besides the above matrices, another one deserves to be mentioned, since it also plays a key role in the mode orthogonalization procedure – it appears in the equilibrium equations of linearised buckling analyses (the so-called “geometric stiffness matrix” – *e.g.*, Schardt 1994) and reads

$$\mathbf{X}_{ij} = \int_S \sigma_{xx}^M t (\bar{v}_i \bar{v}_j + \bar{w}_i \bar{w}_j) dy \tag{7}$$

where σ_{xx}^M are the pre-buckling longitudinal normal stresses.

3. Steel-concrete composite bridge analysis

3.1 Introduction

The procedures involved in a GBT-based structural analysis of steel-concrete composite bridges are illustrated next, through their application to bridges exhibiting the two cross-sections shown in Figs. 2 (a₁) - (a₂), namely a twin box-girder section and a twin I-girder section. Both cross-sections comprise a C50/60 concrete deck ($E = 37$ GPa, $\nu = 0.1$) and steel girders ($E = 210$ GPa, $\nu = 0.3$). The twin box-girder cross-section serves the purpose of illustrating (i) the potential of the GBT analyses when applied to complex cross-sections (combining closed cells and open branches) that are susceptible to significant torsional/distortional coupling and (ii) how to allow for the presence of discrete box diaphragms. On the other hand, the twin I-girder cross-section was chosen in order to demonstrate the versatility of the GBT approach whenever it is possible to take advantage of the cross-section symmetric/anti-symmetric behaviour – in such cases, the number of cross-section deformation modes included in the analysis may be substantially reduced, leading to significant computational savings. For illustrative purposes, only twin I-girder symmetric behaviour is dealt with in this work and, therefore, the cross-section is analysed accordingly (see Fig. 2(b₂)) and the corresponding discussion, which is presented in subsection 3.2).

In the next subsections, various specific aspects of a GBT-based structural analysis of steel-concrete composite bridges are addressed individually. One begins by discussing the GBT cross-section

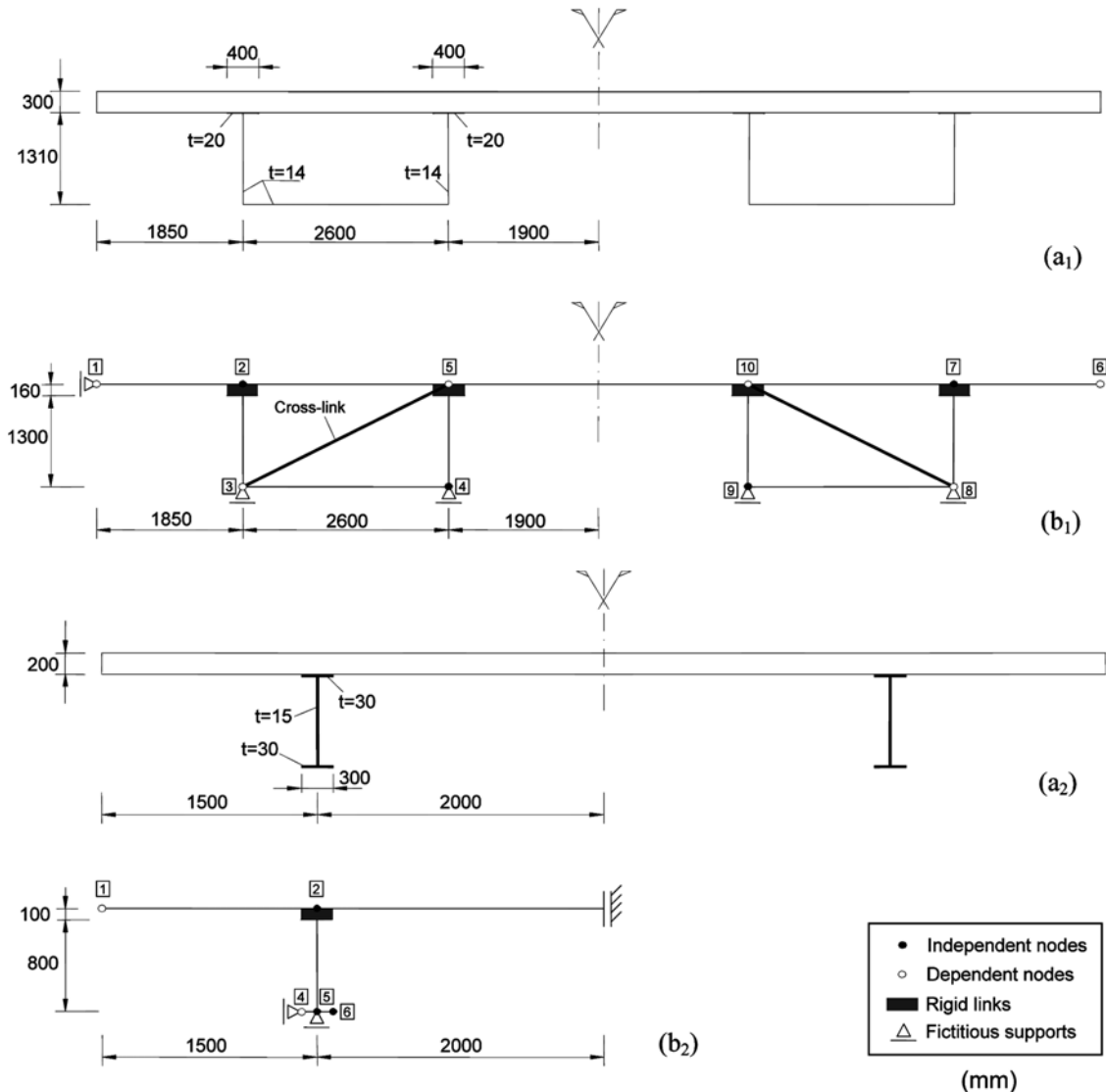


Fig. 2 Bridge box-girder and I-girder cross-sections (a) geometry and (b) GBT discretisation

analysis, which enables the determination of an appropriate set of deformation modes. Next, the linear static analysis of the box-girder bridge is addressed, making due allowance for the presence of cross-section diaphragms discretely located along the girder length. Then, issues related to the capture of shear lag and shear connection flexibility effects are dealt with, which makes it necessary to include some new and non-standard deformation modes. Finally, the last two subsections include the calculation of (i) undamped natural frequencies and associated vibration mode shapes and (ii) critical lateral-torsional-distortional buckling moments and mode shapes. In each case, the GBT-based results are validated through comparisons with values yielded either (i) by shell finite element analyses, carried out with the code ADINA (Bathe 2003) or, only for buckling results, (ii) by finite strip analyses performed with the CUFSM freely available software (Schafer 2003).

3.2 Cross-section analysis

The GBT cross-section analysis is the process leading to the determination of the cross-section deformation mode set, which must be able to describe the beam kinematics with “sufficient accuracy” for the particular problem under consideration – therefore, different problems may require the consideration of distinct deformation mode sets for the same cross-section. This subsection addresses the calculation of the deformation mode sets, concerning the cross-sections depicted in Figs. 2(a₁)-(a₂), that are generally required for any type of structural analysis, *i.e.*, the “fundamental” mode sets. Recently, the authors discussed this subject and proposed a new and general procedure for arbitrary cross-sections, which is capable of handling complex constraints, such as those associated with the presence of box diaphragms (Gonçalves *et al.* 2010b). This general procedure is pursued in this paper and, thus, the following steps are sequentially performed:

- Step - 1 The cross-sections are “reduced” to the walls mid-lines, as shown in Fig. 2(b) and rigid links connecting the steel girder top flanges to the nearest concrete deck nodes are added. The figures show the so-called “cross-section natural nodes” (“independent” and “dependent”-see discussion below), which correspond to wall intersections/outstands and are used to generate the cross-section warping deformation modes. Wall transverse inextensibility is assumed ($\epsilon_{yy}^M = 0$, as customary in most GBT analyses²) and, thus, the in-plane constraint introduced by the cross-section diaphragms (i) may be modeled through a single rigid cross-link in each box-girder section cell and (ii) is implicitly allowed by the I-girder cross-section discretisation, due to the disposition of the fictitious lateral supports (see the next step).
- Step 2 - The so-called “conventional” or “Vlasov” GBT deformation modes are calculated by assuming zero membrane shear deformability ($\gamma_{xy}^M = 0$ – “Vlasov’s assumption”) and imposing warping (\bar{u}) displacements at the cross-section natural nodes. In order to achieve this goal, one must first define the auxiliary “frame” systems depicted in Fig. 2(b), where the independent \bar{v} wall displacements are prevented by fictitious lateral supports – note that the box-girder section involves 5 supports and the I-girder section only 2. Then, the proposed general procedure makes it possible to identify the cross-section “independent natural nodes”, *i.e.*, the set of natural nodes capable of generating compatible and independent warping functions. The box-girder cross-section has only 4 independent nodes (an appropriate set of such nodes is, for instance, {2,4,7,9}), whereas the I-girder cross-section has only 3 independent nodes (the selected set may be {2,5,6}). The imposition of warping displacements at each one of these nodes generates the conventional mode set, with a total of 4 modes for the box-girder section and 3 modes for the I-girder section.
- Step 3 - The conventional modes are orthogonalised, thus making it possible to retrieve the classic prismatic beam theory cross-section modes (the so-called “rigid-body” modes: axial extension, major/minor axis bending and torsion about the shear centre). As originally proposed by Schardt (1989), this is achieved by solving three auxiliary eigenvalue problems involving pairs of the GBT modal matrices (6)-(7). However, for cross-sections with closed cells, such as the twin box-girder section, one must first add a shear deformation mode that causes a shear flow in the closed cells equal to that associated with the classic torsional mode in thin-

²As already mentioned in section 2, this assumption may not be acceptable for some particular problems. For instance, (i) Silvestre and Camotim (2003) used linear transverse extension modes to capture the post-buckling behaviour of thin-walled members and (ii) Gonçalves *et al.* (2010b) employed linear and quadratic modes to analyze the large displacement behaviour of thin-walled members.

walled beam theory. For multi-cell cross-sections, the calculation of this shear flow generally requires solving a system of equations (*e.g.*, Murray 1986) – however, since the twin box-girder dealt with here is symmetric, it can be immediately recognised that the shear flow must be the same in both cells. This procedure leads to the first 5 modes shown in Fig. 3(a): axial extension (1), major/minor axis bending (2, 3), torsion about the shear centre (4) and distortion (5). For the I-girder section, the symmetric support conditions prevent the occurrence of rigid-body torsion and, thus, one is led to the first 3 modes depicted in Fig. 3(b): axial extension (1), minor axis bending (2) and distortion (3).

Step 4 - In the box-girder cross-section, unit extensions ($e = 1$) are imposed in each cross-link, while maintaining $\bar{u} = 0$ at the independent nodes and $\gamma_{xy}^M = 0$ in all walls. The distortional modes 6 and 7, shown in Fig. 3(a), are obtained from this reasoning and correspond to the occurrence of symmetric and anti-symmetric extensions in the cross-links. Although it is possible to orthogonalise the ensuing warping functions with respect to those associated with the first 5 modes (Gonçalves *et al.* 2010b), this is not an essential step and, thus, it is not pursued in this paper. Note that, in the I-girder section, the “equivalent” $e = 1$ mode is the (already calculated) distortional mode 3 (see Fig. 3(b)).

Step 5 - Finally, in order to improve the accuracy of the GBT analyses, membrane shear deformation is allowed for in some selected walls, by imposing $\gamma_{xy}^M = 1$ at each of them while keeping $\gamma_{xy}^M = 0$ in the remaining ones, $e = 0$ at the rigid links and $\bar{u} = 0$ at the independent nodes. While all the steel walls are selected in the box-girder section³, in the I-girder section the selection is restricted to the steel web. Then, a simple combination of symmetric and anti-symmetric shapes⁴ leads to modes 8-13 in Fig. 3(a) (note that mode 8 is associated with vertical shear) and to mode 4 in Fig. 3(b).

One final word to stress again that the GBT cross-section analysis procedure is fully capable of obtaining additional deformation modes and, more importantly, modes with different kinematic characteristics. This is generally achieved by (i) relaxing some of the fundamental hypotheses concerning the strains ($\varepsilon_{yy}^M = 0$ and/or $\gamma_{xy}^M = 0$, leading to “transverse extension modes” and the previously addressed “shear deformation modes”) or by (ii) adding cross-section nodes, located between the natural nodes (*i.e.*, along the wall mid-lines – the so-called “intermediate nodes”). However, in the illustrative examples presented in this work, such additional deformation modes will only be included in the GBT analysis when their presence is indispensable to obtain accurate results.

3.3 Linear (first-order) static analysis

Consider a simply supported 20 m span bridge with the twin box-girder cross-section shown in Fig. 2(a₁), subjected to a mid-span eccentric vertical point load applied at node 2 (see Fig. 2(b₁)) and equal to 1 kN. Two box-girder diaphragm locations are considered, namely (i) only at the piers (Case I) and (ii) both at the piers and at mid-span (Case II). Due to the longitudinal symmetry of the problem, only half of the bridge is analysed. The analysis is carried out by means of a standard GBT-based 2-node Hermitean beam finite element that incorporates the 13 deformation modes shown in Fig. 3(a) - thus, a

³Obviously excluding the top flanges, since they are rigidly attached to the concrete deck. Although one may also include independent shear deformation in the concrete deck, this is clearly unnecessary for most situations.

⁴It is also possible to devise a method to orthogonalise the shear deformation modes (*e.g.*, Gonçalves *et al.* 2010b).

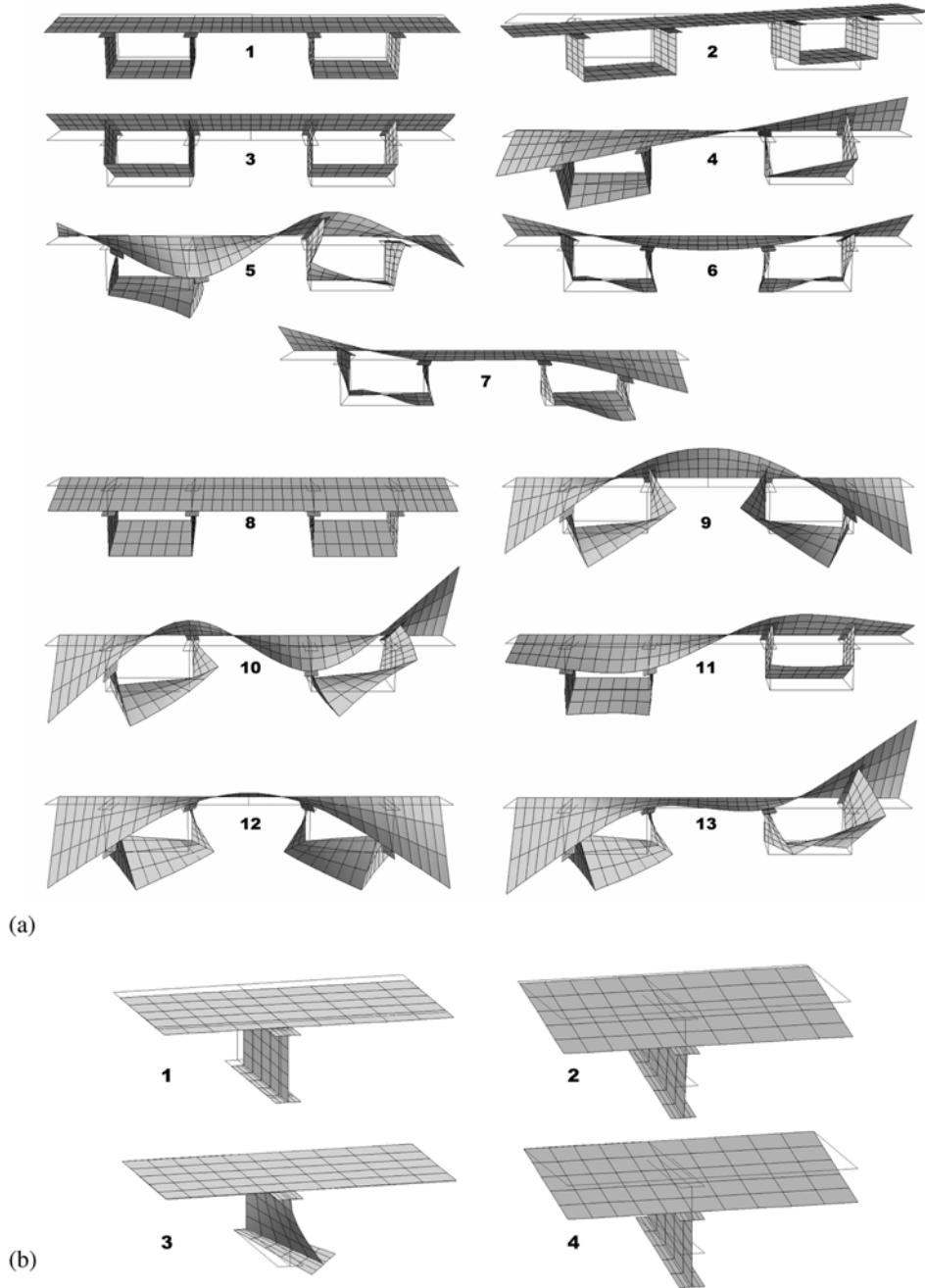


Fig. 3 Deformation modes for the (a) box-girder and (b) I-girder cross-sections

$4 \times 12 + 3 \times 1 = 51$ d.o.f. element stiffness matrix is obtained (recall that a duplicate d.o.f., concerning the axial extension mode, must be removed). The kinematic boundary (support) conditions read

$$\phi_{2-13}(x=0) = 0 \tag{8}$$

$$\phi_{2-13,x}(x=10) = 0 \tag{9}$$

$$\phi_{1,x}(x=10) = 0 \tag{10}$$

$$\phi_{6-7}(x=10) = 0 \tag{11}$$

where the last equation concerns diaphragms located at mid-span and, therefore, applies only to Case II. For comparison purposes, a 4-node shell finite element analysis was also performed in ADINA, adopting the mesh⁵ shown in Fig. 5, which involves approximately 3900 d.o.f.

The results obtained are shown in Figs. 4 (vertical displacements at node 2) and 5 (bridge deformed configurations). Fig. 4(a) show the variation of the mid-span vertical displacement with the number of beam finite elements, whereas Fig. 4(b) provide the longitudinal variation, from the left support to mid-span, of the vertical displacement (the GBT-based results were obtained using 3 finite elements). It is worth noting that the GBT-based results shown in these figures include *modal participations*, i.e., the contributions of each relevant deformation mode to the vertical displacement. The observation of these

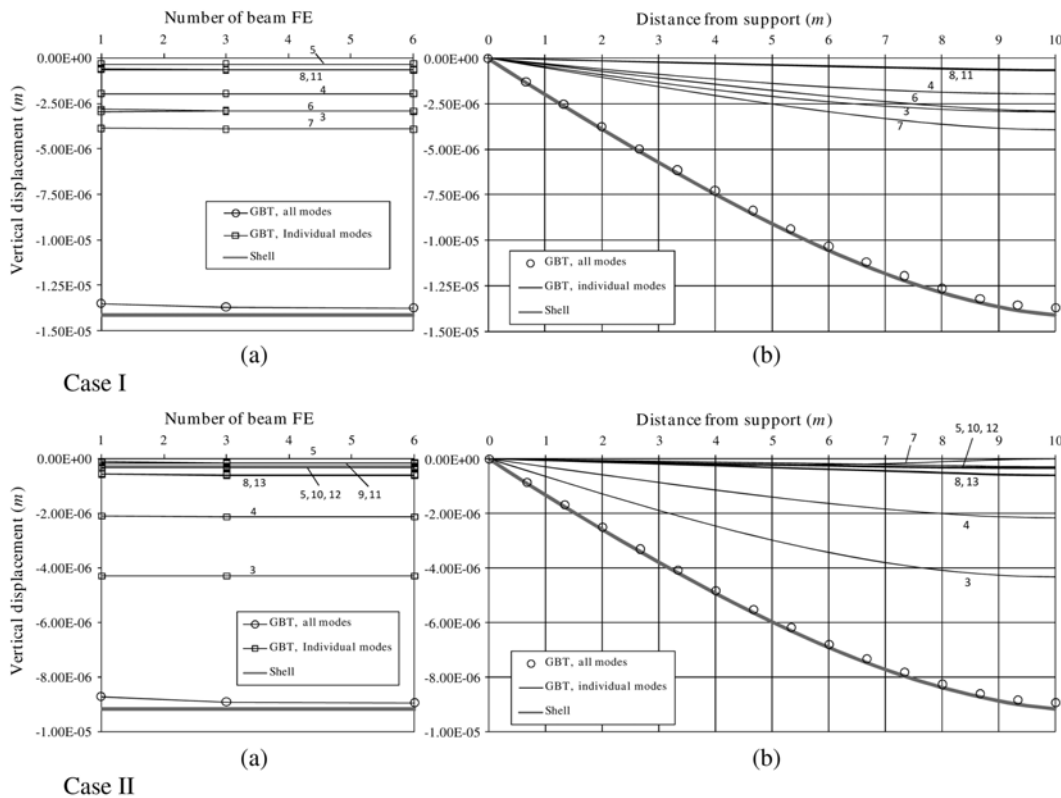


Fig. 4 (a) Vertical displacement of the point of load application vs. number of beam finite elements and (b) longitudinal variation of the vertical displacement of node 2 (Cases I and II)

⁵Actually, beam elements were also included in the ADINA finite element model, in order to simulate the steel girder top flanges. Moreover, rigid elements were employed to materialise (i) the discrete box diaphragms and (ii) the connection between the steel top flanges and the concrete deck.

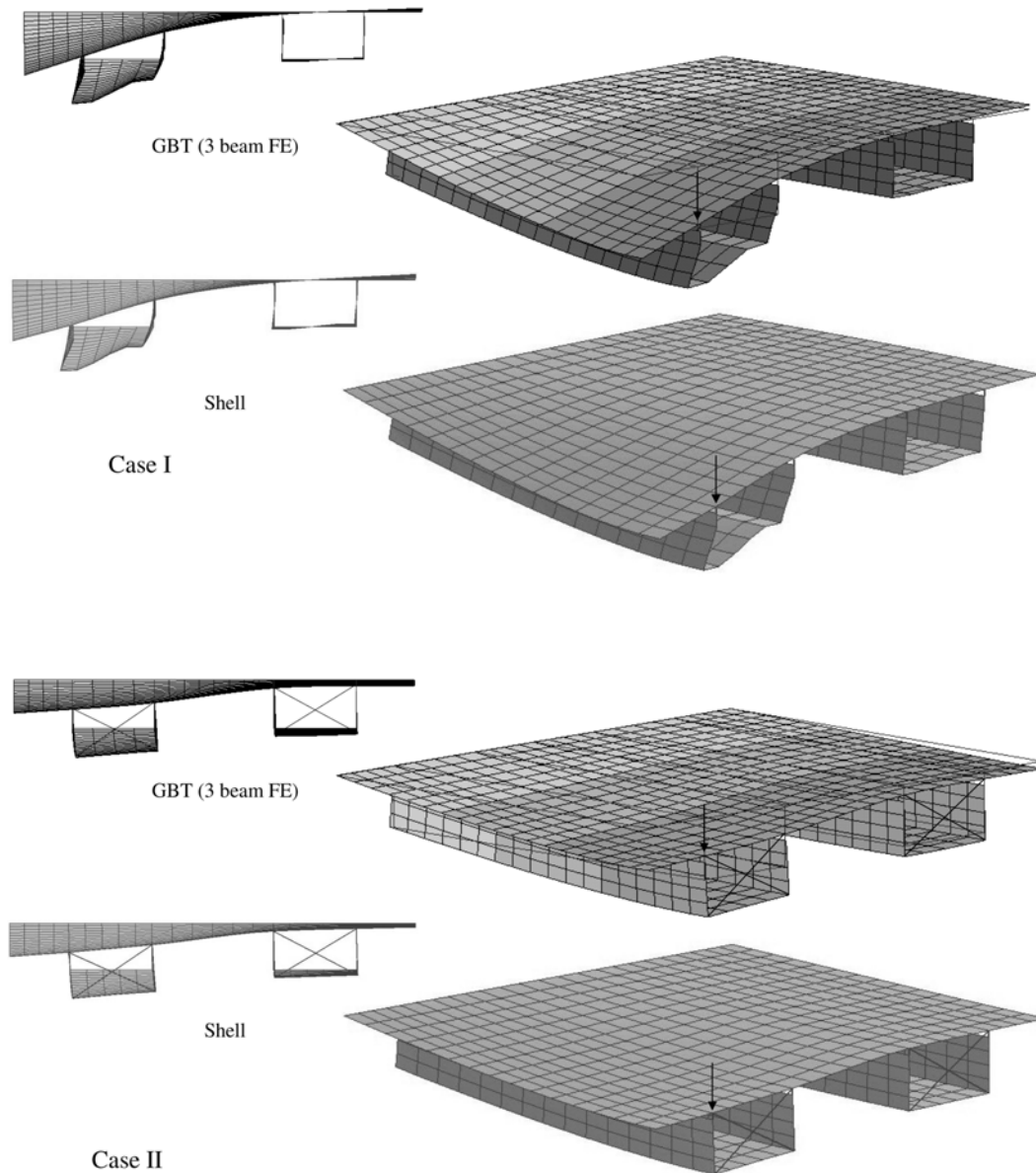


Fig. 5 Deformed configurations ($\times 10^5$) of half of the box-girder bridge with diaphragms located only at the piers (Case I) and both at the piers and at mid span (Case II)

results prompts the following remarks:

- (i) The plots presented in Fig. 4(a) make it possible to conclude that there is no advantage in adopting a longitudinal discretisation involving more than 3 beam finite elements. Indeed, employing 6 finite elements does not lead to a significant further reduction of the difference with respect to the shell model, which is already below 3%. Moreover, the GBT modal participations provide valuable insight into the mechanics of the bridge structural response – no such detailed and

- structurally meaningful information can be extracted from the shell finite element results. For instance, one readily concludes that the bridge behaviour combines bending (3), torsion (4) and $e = 1$ distortion (6 + 7) and that the contributions of the $e = 1$ distortional modes are virtually eliminated by including the mid-span diaphragms (Case II).
- (ii) Concerning Fig. 4(b), it can be observed that the most significant differences between the two models take place at mid-span (although below 3%, as discussed in the previous item), providing evidence of the occurrence of localised web deformation in this region. In fact, if the mid-span displacements are measured at node 3 (see Fig. 2(b₁)), the differences fall to 1.2% (Case I) and 0.7% (Case II), showing that wall transverse membrane extensions ε_{yy}^M are involved. In order to capture this effect, it would be necessary to include “transverse extension modes” in the analysis.
 - (iii) The comparison between the pairs of bridge deformed configurations depicted in Fig. 5, yielded by the beam and shell finite element models, clearly illustrate the potential of the GBT-based analyses. Indeed, in spite of the huge difference between the numbers of d.o.f. involved in each model (e.g., in Case I the GBT analysis involves just 84 d.o.f.), they lead to remarkably similar deformed configurations.

3.4 Shear lag

Shear lag is a phenomenon that often arises in wide flange beams and stems from membrane shear deformation. In order to capture such phenomenon accurately, it is indispensable to include in the GBT analysis shear deformation modes allowing for both uniform and non-uniform shear deformation in the relevant walls. However, note that, since wall transverse inextensibility is generally assumed ($\varepsilon_{yy}^M = 0$, i.e., $\bar{v}(y) = \text{constant}$), the shear lag deformation modes cannot be generated by \bar{v} functions, but rather by \bar{u} (warping) functions. In the traditional GBT approach, non-uniform warping in a given wall is accounted for by considering intermediate nodes in that wall, which generate warping deformation modes associated with piecewise linear warping functions (e.g., Möller 1982, Silvestre and Camotim, 2003). However, it is obviously possible to adopt different interpolating functions, namely sinusoidal functions (e.g., Gonçalves *et al.* 2010b) – this approach will be applied next to analyse the box-girder and I-girder bridges.

In the box-girder bridge, the aim is to capture shear lag in the steel bottom flanges. Since constant shear strains were already accounted for by deformation modes 8-13 (see Fig. 3(a)), one just needs to include the non-uniform component and, for this particular example, only single half-wave sinusoidal warping modes in each bottom flange are considered, leading to the two modes shown in Fig. 6(a). Returning to the bridge analysed in the previous subsection, Fig. 6(b) shows the mid-span longitudinal normal stresses at the box-girder cross-section where the load is applied, for Cases I and II, obtained with (i) the (previous) GBT analyses, including modes 1-13 and 3 beam elements, (ii) GBT analyses including modes 1-15 and also 3 beam elements and (iii) the shell element models. It is clear that the inclusion of the shear lag modes (14,15) improves the accuracy of the GBT-based results and makes it possible to capture quite reasonably the bottom flange non-linear stress distribution. Note, however, that in Case II additional deformation modes would be required to reach the 78.6 kPa peak stress yielded by the shell FE model, currently underestimated by about 17%.

In the I-girder section, one studies the shear lag in the concrete deck. Since no deck shear deformation is accounted for by the deformation modes shown in Fig. 3(b), both linear and sinusoidal (with increasing half-wave numbers) warping modes are added – Fig. 7(a) shows the shapes of the first 6 modes.

The analysis is carried out for a simply supported 8 m span bridge, acted by two sinusoidal line loads

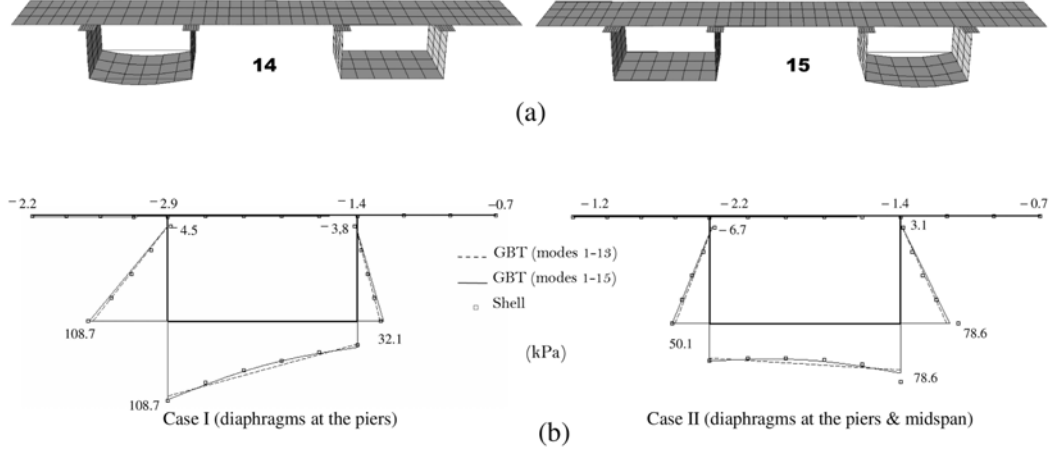


Fig. 6 (a) Shear lag deformation modes and (b) mid span longitudinal normal stress distribution at the box girder where the load is applied (values correspond to the shell FE model)

$q(x) = \sin(\pi x / L)$ (kN/m) applied on top of each steel web (node 2). For this particular loading, the problem exact solutions are of the form $\phi_k(x) = \bar{\phi}_k \sin(\pi x / L)$, whrer $\bar{\phi}_k$ are the deformation mode amplitudes (the problem unknowns), and the equilibrium equation system becomes

$$\left(\frac{\pi^4}{L^4} [\mathbf{C}] + \frac{\pi^2}{L^2} [\mathbf{D}] + [\mathbf{B}] \right) \begin{bmatrix} \bar{\phi}_1 \\ \vdots \\ \bar{\phi}_D \end{bmatrix} \sin\left(\frac{\pi x}{L}\right) = \begin{bmatrix} \bar{q}_1 \\ \vdots \\ \bar{q}_D \end{bmatrix} \sin\left(\frac{\pi x}{L}\right) \quad (12)$$

where $\mathbf{D} = \mathbf{D}_1 - (\mathbf{D}_2^1 + \mathbf{D}_2)$ and $\bar{q}_k = \bar{q}_x \bar{u}_k + \bar{q}_y \bar{v}_k + \bar{q}_z \bar{w}_k$ are the modal forces (the loading is deemed applied at the wall mid-surface). Note that the dimension of the equation system is equal to the number of deformation modes D , which means that significant computational savings are achieved.

Fig. 7(b) shows the mid-span longitudinal normal stresses in the concrete deck, obtained with (i) a GBT analysis, using either 0 or 8 shear lag modes (*i.e.*, a 4 or 12 d.o.f. system, respectively), and (ii) a 9-node shell finite element analysis involving the discretisation depicted in Fig. 7(c) (due to symmetry, only a quarter of the bridge is analysed). One observes that shear lag has a marked influence on the normal stress distribution and it is clear that there is an excellent agreement between the two models when the shear lag deformation modes are included in the GBT analysis, in spite of the huge disparity in the numbers of d.o.f. involved (3600 vs. 12).

3.5 Shear connection flexibility

The deformation modes that account for the flexibility of the shear connection are obtained by (i) removing the rigid links depicted Figs. 2(b) and (ii) imposing unit longitudinal slips in each steel - concrete interface, while simultaneously enforcing $\epsilon_{yy}^M = \gamma_{xy}^M = 0$ in all cross-section walls and $\bar{u} = 0$ at all independent nodes. The imposition of the unit longitudinal slip causes cross-section warping that, due to

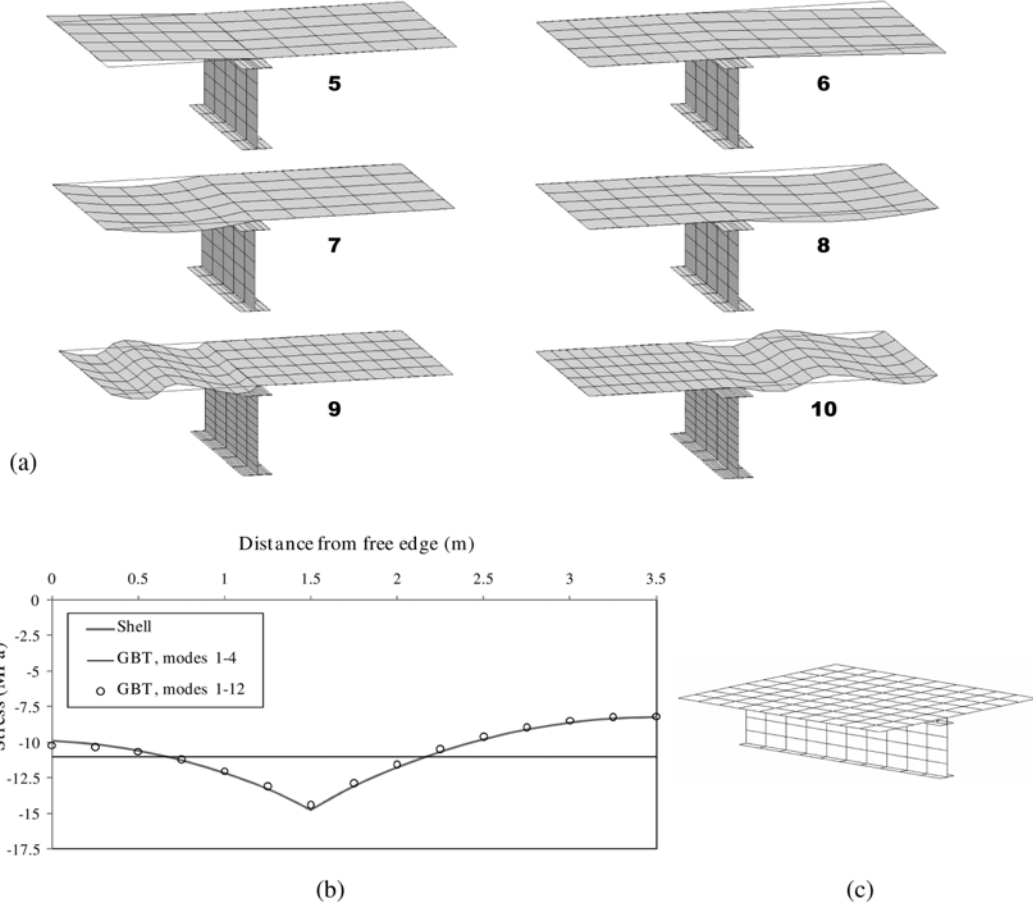


Fig. 7 I-girder bridge (a) first 6 shear lag deformation modes, (b) mid-span normal stress distribution in the concrete deck and (c) 9-node shell element model

the imposed constraints, generally leads to non-null \bar{v} and \bar{w} wall displacements, which are calculated in the usual way. For the sake of illustration, Fig. 8(a) shows the “longitudinal slip deformation mode” (16) associated with the imposition of a unit slip at node 2 of the box-girder cross-section.

The internal virtual work must now include the work done by the longitudinal shear force along the steel-concrete interface, which reads

$$\delta W_{int} = - \int_L \sum_i f^i(x) \delta s^i(x) dx \quad (13)$$

where f^i and s^i are the longitudinal shear force and work-conjugate slip along shear connection i . According to the GBT kinematic description, the slip may be expressed as a function of the modal amplitude functions

$$s^i(x) = \sum_k \bar{s}_k^i \phi_{k,x}(x) \quad (14)$$

where \bar{s}_k^i is the modal slip along connection i for mode k . For a constant shear connection stiffness κ^i , one has

$$f^i(x) = \kappa^i s^i(x) = \sum_i \kappa^i \bar{s}_k^i \phi_{k,x}(x) \quad (15)$$

and it is possible to write

$$\delta W_{int} = -\sum_k \int_L [\delta \phi_{,x}]^t [\kappa^i] [\phi_{,x}] dx \quad (16)$$

with the new modal matrix given by

$$[\kappa^i]_{jk} = \kappa^i \bar{s}_j^i \bar{s}_k^i \quad (17)$$

If each longitudinal slip deformation mode corresponds to a unit slip in a single shear connection, then the above matrix is diagonal with $[\kappa^i]_{jj} = \kappa^i$.

For illustrative purposes, one investigates the influence of the (constant) shear connection flexibility associated with mode 16 (slip at node 2 only – see Fig. 8(a)), for the bridge with diaphragms at the piers (Case I). As before, the bridge is acted by a mid-span eccentric vertical load equal to 1 kN applied at node 2. Fig. 8(b) shows the variation of the vertical displacement at the point of load application with the shear connection stiffness (in logarithmic scale), obtained with the GBT-based beam FE, including modes 1-13 and 16, and the shell FE model. It is clear that the inclusion of mode 16 leads to a virtually perfect capture of the shear connection flexibility effect, even when just 1 beam finite element is considered. Moreover, these results make it possible to conclude that the influence of the shear connection stiffness is only relevant for $1E3 < \kappa < 1E7$ kN/m² – outside this range, the vertical displacement varies less than 1%. Finally, it is still worth mentioning that the vertical displacement shown in Fig. 4(a), concerning Case I, is obviously recovered for $\kappa > 1E7$ kN/m².

3.6 Free vibration analysis - undamped natural frequencies

Thin-walled beam vibration analysis is a long-established field of application of GBT (*e.g.*, Saal 1974, Schardt and Heinz 1991, Camotim *et al.* 2007, Bebiano *et al.* 2008). The dynamic equilibrium equations are obtained from Hamilton's Principle and the member undamped natural frequencies ω can be determined by solving the homogeneous form of the equations. For simply supported members, the problem exact solutions correspond to sinusoidal amplitude functions $\phi_k(x) = \bar{\phi}_k \sin(n\pi x/L)$, where $\bar{\phi}_k$ and n are the modal participations and longitudinal half-wave number of the free vibration mode shapes. The dimension of the GBT equilibrium equation system is again equal to the number of deformation modes included in the analysis, D , and reads

$$\left(\left(\frac{n\pi}{L} \right)^4 [\mathbf{C}] + \left(\frac{n\pi}{L} \right)^2 [\mathbf{D}] + [\mathbf{B}] - \omega^2 \left([\mathbf{R}] + \left(\frac{n\pi}{L} \right)^2 [\mathbf{Q}] \right) \right) \begin{bmatrix} \bar{\phi}_1 \\ \vdots \\ \bar{\phi}_D \end{bmatrix} \sin\left(\frac{n\pi x}{L}\right) = \begin{bmatrix} 0 \\ \vdots \\ 0 \end{bmatrix} \quad (18)$$

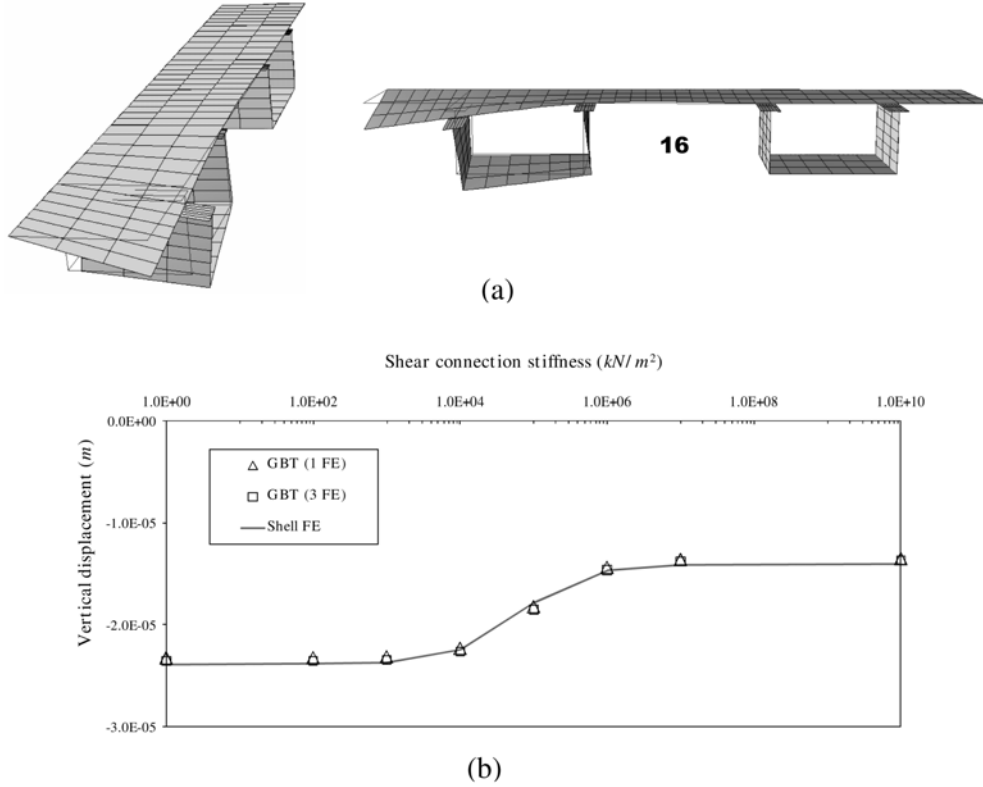


Fig. 8 (a) Longitudinal slip deformation mode 16 and (b) variation of the vertical displacement at the point of load application with the shear connection stiffness

where the new modal mass matrices are given by

$$\mathbf{Q}_{ij} = \mathbf{Q}_{ij}^M + \mathbf{Q}_{ij}^B = \int_S \rho t \bar{u}_i \bar{u}_j dy + \int_S \frac{\rho t^3}{12} \bar{w}_i \bar{w}_j dy \quad (19)$$

$$\mathbf{R}_{ij} = \mathbf{R}_{ij}^M + \mathbf{R}_{ij}^B = \int_S \rho t (\bar{v}_i \bar{v}_j + \bar{w}_i \bar{w}_j) dy + \int_S \frac{\rho t^3}{12} \bar{w}_{i,y} \bar{w}_{j,y} dy \quad (20)$$

and ρ is the mass per unit volume, taken as 77/9.81 for steel and 25/9.81 for concrete (in ton/m³).

For the box-girder bridge under consideration, it will be shown next that accurate results (undamped natural frequencies and corresponding vibration mode shapes) can only be achieved through the inclusion of “local-plate” deformation modes associated with the transverse bending of the slender lower flanges. According to the standard GBT procedure, such deformation modes are obtained by first introducing intermediate nodes within the walls (the lower flanges, in this case) and then imposing $\bar{w} = 1$ displacements at these nodes. However, the approach followed in this work, which was already employed for the shear lag deformation modes, consists of determining appropriate local-plate

deformation modes *without* resorting to intermediate nodes. The first two modes are obtained by imposing symmetric/anti-symmetric *rotations* at nodes 3, 4, 8, 9 (see Fig. 2(b₁)), thus leading to modes 17-18 shown in Fig. 9(a). As for modes 19-20, they correspond to symmetric and anti-symmetric configurations associated with the shape function $\bar{w}(y) = 1 - \cos(2\pi y/b)$ in each lower flange, where b is the flange width⁶. If additional modes were required to enhance the accuracy of the results, sinusoidal functions with more half-waves should be also considered.

Fig. 9(b) and Table 1 concern the first two (longitudinally) symmetric vibration mode shapes and the corresponding natural frequencies, obtained for Case I (diaphragms only at the piers) by means of (18) (with three deformation mode sets) and a shell FE analysis. The natural frequencies given in Table 1 make it possible to assess the relevance of including the local-plate deformation modes 17-20 in the GBT analysis – it is clearly shown that including the four modes brings the GBT-based natural frequencies much closer to the values yielded by the shell FE model. Fig. 9(b) compares the bridge vibration mode shapes provided by the two models (the GBT-based shapes are obtained with 17 modes: 1-13 and 17-20) and a virtually perfect match is observed, even if the GBT analysis involves merely solving a 17 d.o.f. eigenvalue problem of the form (18).

3.7 Buckling (bifurcation) analysis

Finally, one addresses the calculation of critical moments in steel-concrete composite beams. It is

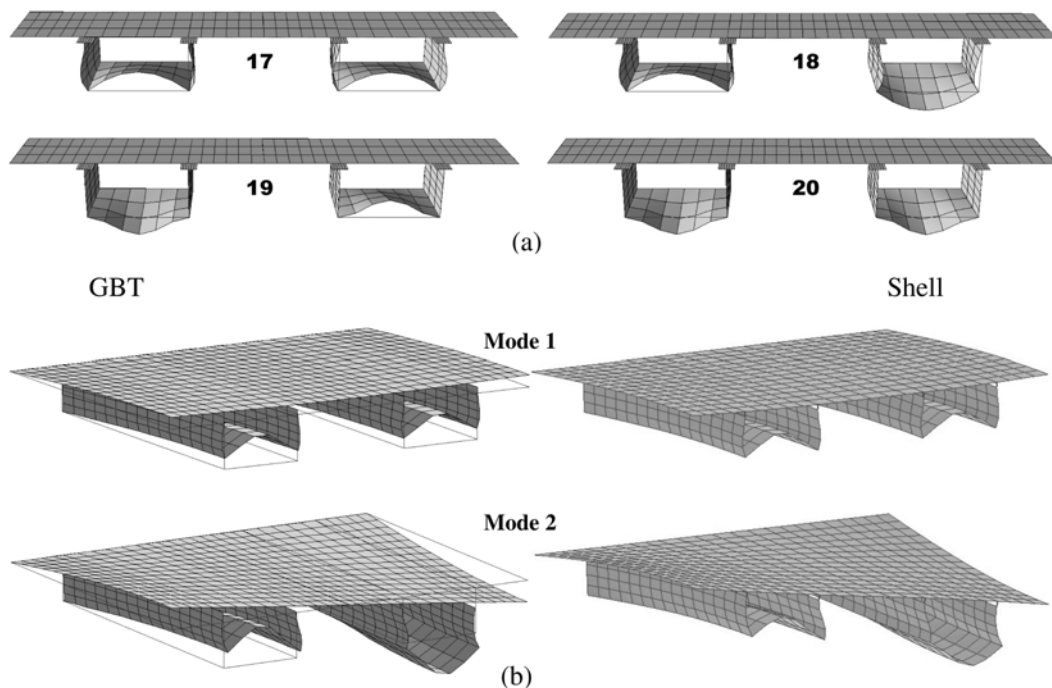


Fig. 9 Box-girder bridge (a) local-plate deformation modes 17-20 and (b) shapes of the first two symmetric vibration modes

⁶Note that this function satisfies the boundary conditions $\bar{w}(0) = \bar{w}(b) = \bar{w}_{,y}(0) = \bar{w}_{,y}(b) = 0$.

Table 1 Box-girder bridge natural frequencies

Type of model	Natural frequencies (Hz)	
	Mode 1	Mode 2
GBT, modes 1-13	6.89	7.23
GBT, modes 1-13 and 17-18	6.82	7.17
GBT, modes 1-13 and 17-20	6.70	7.03
Shell FE model	6.67	6.86

well known that such beams may be susceptible to buckling phenomena in hogging bending regions and that the associated buckling mode shape involves cross-section in-plane distortion – hence, this type of instability is sometimes designated as *lateral-torsional-distortional* buckling. The presence of cross-section distortion makes it somewhat difficult to obtain accurate buckling solutions on the basis of classic prismatic bar theory, but it poses no problems for GBT.

For illustrative purposes, one analyses simply supported bridges with the double I-girder cross-section shown in Fig. 2(a₂) and subjected to uniform hogging bending (thus, there are no shear lag effects). The deck is assumed fully cracked/uncracked in the longitudinal/transverse directions, respectively, and the concrete longitudinal tensile strength is neglected. It is also assumed that a steel reinforcement area equal to 7.854 cm²/m exists at the concrete deck mid-line. In this simple problem, sinusoidal amplitude functions $\phi_k(x) = \bar{\phi}_k \sin(n\pi x/L)$ constitute once more exact solutions ($\bar{\phi}_k$ and n are now the modal participations and longitudinal half-wave number of the buckling mode) and the GBT buckling equations read (e.g., Gonçalves *et al.* 2009)

$$\left(\left(\frac{n\pi}{L} \right)^4 [\mathbf{C}] + \left(\frac{n\pi}{L} \right)^2 [\mathbf{D}] + [\mathbf{B}] + \lambda \left(\frac{n\pi}{L} \right)^2 [\mathbf{X}] \right) \begin{bmatrix} \bar{\phi}_1 \\ \vdots \\ \bar{\phi}_D \end{bmatrix} \sin\left(\frac{n\pi x}{L}\right) = \begin{bmatrix} 0 \\ \vdots \\ 0 \end{bmatrix} \quad (21)$$

where $\lambda = M_{cr}/M$ is the critical load parameter and M is the applied moment for which \mathbf{X} is calculated (see Eq. (7)). Note that a mere D -dimensional system is obtained, where D is again the number of deformation modes included in the analysis.

Since this bridge constitutes a classic “inverted U-frame” (e.g., Johnson and Anderson 2004), the symmetry simplification displayed in Fig. 2(b₂) can be adopted and, therefore, the corresponding deformation modes (1-4 in Fig. 3(b)) apply. It is obvious that, out of this set of deformation modes, only the distortional mode 3 needs to be included in the buckling analysis. This rather interesting feature stems directly from the fact that one is employing a “fundamental” deformation mode set with only four modes, *i.e.*, from the fact that the modes were obtained by assuming several kinematic constraints (namely $\varepsilon_{yy}^M = \gamma_{xy}^M = 0$) and no intermediate nodes. Although the inclusion of more deformation modes, due to either relaxing the kinematic constraints or adding intermediate nodes, will certainly improve the results, one of the most appealing features of GBT resides in the fact that the “fundamental” GBT deformation mode set already constitutes a suitable base to describe quite accurately the beam kinematics for a wide range of problems⁷.

For single deformation mode (3) buckling, (21) yields the closed-form solution

$$\lambda = \frac{M_{cr}}{M} = \frac{-1}{\mathbf{X}_{33}} \left(\left(\frac{n\pi}{L} \right)^2 \mathbf{C}_{33} + \mathbf{D}_{33} + \left(\frac{L}{n\pi} \right)^2 \mathbf{B}_{33} \right) \quad (22)$$

and, as shown by Schardt (1994), the minimum critical moment corresponds to

$$\frac{M_{cr}}{M} = -\frac{\mathbf{D}_{33} + 2\sqrt{\mathbf{B}_{33}\mathbf{C}_{33}}}{\mathbf{X}_{33}} \quad (23)$$

and occurs for a beam length equal to

$$L = n\pi \sqrt[4]{\mathbf{C}_{33}/\mathbf{B}_{33}} \quad (24)$$

Fig. 10(a) provides the variation of M_{cr} with L , obtained by means of (22) and the use of the finite strip code CUFSM (Schafer 2003). There is a virtually perfect match, which means that no additional deformation modes need to be included in the GBT buckling analyses. Finally, Fig. 10(b) depicts the buckling mode shape obtained with GBT for the $L = 8$ m beam, which corresponds to single half-wave buckling ($n = 1$).

4. Conclusions

This paper reported recent developments concerning the application of Generalised Beam Theory (GBT) to the structural analysis of thin-walled steel-concrete composite bridges and its main objective was to provide evidence that the GBT-based analyses (either semi-analytical or finite element based) can be considerably more efficient, versatile and insightful than similarly accurate finite strip or shell finite element analyses. In particular, attention is drawn to the following aspects:

- (i) The “fundamental” GBT deformation mode set, generated by means of the procedure proposed by the authors (which does not require resorting to intermediate nodes), makes it possible to obtain accurate solutions for a wide range of problems, namely those involving the bridge linear static, undamped free vibration and buckling (bifurcation) behaviours, and concerning members with complex cross-sections, such as twin box-girder bridges (which combine closed cells with open branches). In particular, this deformation mode set enables the easy capture of the influence of box diaphragms discretely located along the bridge girders length.
- (ii) The inclusion of specific additional deformation modes in the bridge analysis makes it possible to handle accurately phenomena such as shear lag effects in wide flanges or the influence of the shear connection flexibility.
- (iii) The accuracy of the GBT-based results was assessed through comparisons with values yielded by shell finite element (mostly) or finite strip analyses and an excellent agreement was found in all cases.

Future developments, already under way, include (i) the improvement of the material modelling, namely by taking into account non-linear effects for the concrete, and (ii) the inclusion of shrinkage, post-tensioning and temperature effects.

⁷For instance, it is indispensable to add intermediate nodes for the calculation of the cross-section deformation modes when dealing with local-plate buckling problems.

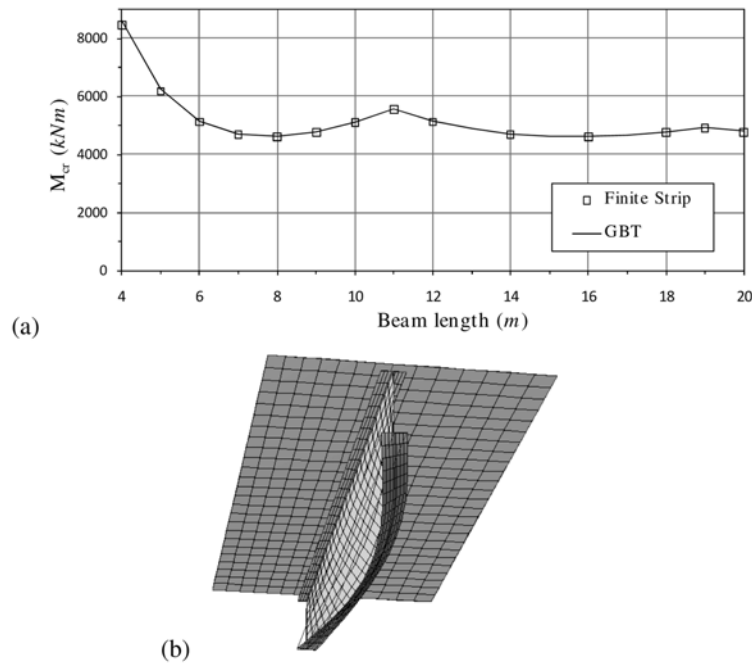


Fig. 10 (a) Variation of M_{cr} with the beam length L and (b) GBT-based critical buckling mode shape for $L = 8$ m

References

- Bathe, K. (2003), *ADINA System*, ADINA R&D Inc.
- Bebiano, R., Silvestre, N. and Camotim, D. (2008), "Local and global vibration of thin-walled members subjected to compression and non-uniform bending", *J. Sound. Vib.*, **315**(3), 509-535.
- Camotim, D., Silvestre, N., Gonçalves, R. and Dinis, P. B. (2004), "GBT analysis of thin-walled members: new formulation and applications", *Thin-Walled Structures: Recent Advances and Future Trends in Thin-Walled Structures Technology*, J. Loughlan (ed.), Canopus Publishing, Bath, 137-168.
- Camotim, D., Silvestre, N. Gonçalves, R. and Dinis, P. B. (2006), "GBT-based structural analysis of thin-walled members: overview, recent progress and future developments", *Adv. Eng. Struct., Mechanics & Construction*, M Pandey, WC Xie, L Xu (eds.), Springer, Dordrecht, 187-204.
- Camotim, D., Silvestre, N. and Bebiano, R. (2007), "GBT local and global vibration analysis of thin-walled members", *Dynamics of Plated Structures: Analysis and Design*, NE Shanmugam, CM Wang (eds.), Woodhead Publishing Limited, Cambridge, 36-76.
- Camotim, D., Basaglia, C. and Silvestre, N. (2010), "Global buckling analysis of thin-walled steel frames: a state-of-the-art report", *Thin. Wall. Struct.* (in press)
- Davies, J. M. (1998), "Generalised beam theory (GBT) for coupled instability problems", *Coupled instabilities in metal structures: theoretical and design aspects*, J Rondal (ed.), Springer-Verlag, 151-223, Austria.
- Gonçalves, R. and Camotim, D. (2004), "GBT local and global buckling analysis of aluminium and stainless steel columns", *Comput. Struct.*, **82**(17-19), 1473-484.
- Gonçalves, R. and Camotim, D. (2007), "Thin-walled member plastic bifurcation analysis using generalized beam theory", *Adv. Eng. Softw.*, **38**(8-9), 637-646.
- Gonçalves, R., Camotim, D. and Ritto-Corrêa, M. (2008), "Steel and composite bridge analysis using generalized beam theory", *Steel Bridges – Advanced Solutions & Technologies (Proceedings of 7th International Conference on Steel Bridges – Guimarães)*, P Cruz, LS Silva, F Schröter (eds.), ECCS, Coimbra, 377-389.

- Gonçalves, R., Dinis, P. B. and Camotim, D. (2006), "Box girder bridge analysis using generalized beam theory", *Proceedings of SDSS 2006 International Colloquium on Stability and Ductility of Steel Structures* (SDSS 2006 Lisboa), D Camotim, N Silvestre, PB Dinis (ed.), IST Press, Lisbon, 1027-1036.
- Gonçalves, R., Dinis, P. B. and Camotim, D. (2009), "GBT formulation to analyse the first-order and buckling behaviour of thin-walled members with arbitrary cross-sections", *Thin. Wall. Struct.*, **47**(5), 583-600.
- Gonçalves, R., Le Grogneq, P. and Camotim, D. (2010a), "GBT-based semi-analytical solutions for the plastic bifurcation of thin-walled members", *Int. J. Solids Struct.*, **47**(1), 34-50.
- Gonçalves, R., Ritto-Corrêa, M. and Camotim, D. (2010b), "A new approach to the calculation of cross-section deformation modes in the framework of Generalized Beam Theory", *Computational Mechanics*, *in press*.
- Johnson, R. P. and Anderson, D. (2004). *Designer's Guide to EN 1994-1-1*, Thomas Telford, London.
- Möller, R. (1982), *Zur Berechnung Prismatischer Strukturen mit Beliebigen nicht Formtreuem Querschnitt*, Institut für Statik, Technische Hochschule Darmstadt.
- Murray, N. W. (1986), *Introduction to the Theory of Thin-Walled Structures*, Clarendon Press, Oxford.
- Saal, G. (1974), *Ein Beitrag zur Schwingungsberechnung von Dünnwandigen, Prismatischen Schalenträgwerken mit Unverzweigtem Querschnitt*, Ph.D. Dissertation, Technische Hochschule Darmstadt, Germany. (in German)
- Schafer, B. W. (2003), *CUFSM 2.6, Finite Strip Buckling Analysis of Thin-Walled Members*, Civil Engineering Department, Johns Hopkins University, Baltimore. (www.ce.jhu.edu/bschafer)
- Schardt, R. (1989), *Verallgemeinerte Technische Biegetheorie*, Springer-Verlag, Berlin. (in German)
- Schardt, R. (1994), "Generalized beam theory-an adequate method for coupled stability problems", *Thin. Wall. Struct.*, **19**(2-4), 161-180.
- Schardt, R. and Heinz, D. (1991), "Vibrations of thin-walled prismatic structures under simultaneous static load using generalized beam theory", *Structural Dynamics*, W. Kratzig *et al.* (eds.), Balkema, Rotterdam, 921-927.
- Silvestre, N. and Camotim, D. (2003), "Non-linear generalised beam theory for cold-formed steel members", *Int. J. Struct. Stab. Dy.*, **3**(4), 461-490.
- Silvestre, N. and Camotim, D. (2004), "Distortional buckling formulae for cold-formed steel C and Z section members: part I -derivation", *Thin. Wall. Struct.*, **42**(11), 1567-1597.